Sensors & Actuators: A. Physical 344 (2022) 113756

Contents lists available at ScienceDirect

Sensors and Actuators: A. Physical

journal homepage: www.journals.elsevier.com/sensors-and-actuators-a-physical

Characterization of transient rheological behavior of soft materials using ferrofluid droplets

Danyil Azarkh [a], Melanie Geiger [a], Se-Hyeong Jung [b,c], Erik Noetzel [d], Rudolf Merkel [d], Andrij Pich [b,c,e], Uwe Schnakenberg [a,*]

[a] Institute of Materials in Electrical Engineering 1 (IWE1), RWTH Aachen University, Sommerfeldstraße 24, Aachen 52074, Germany
[b] DWI, Leibniz-Institute for Interactive Materials, Forckenbeckstraße 50, Aachen 52074, Germany
[c] Institute of Technical and Macromolecular Chemistry, RWTH Aachen University, Worringerweg 2, Aachen 52074, Germany
[d] Institute of Biological Information Processing (IBI-2), Mechanobiology, Forschungszentrum Jülich GmbH, Leo-Brandt-Strasse, Jülich 52425, Germany
[e] Aachen Maastricht Institute for Biobased Materials (AMIBM), Maastricht University, Brightlands Chemelot Campus, Urmonderbaan 22, Geleen 6167 RD, the Netherlands

ARTICLE INFO

Keywords:
Ferrofluid droplet
Rheology
Viscoelasticity
Polyacrylamide
Magnetic Bond number
Interfacial tension

ABSTRACT

Physical material properties, such as elasticity, viscosity, or viscoelasticity, can be characterized by using rheometers or stick-type solenoid electromagnets. In this work, we developed a magnet measurement setup based on a Helmholtz arrangement of electromagnets. While applying homogeneous magnet fields to ferrofluid droplets inside a soft material of interest, the deformations of the ellipsoidal deformed droplets were measured. Kelvin-Voigt models and corresponding analytical descriptions were used to calculate the values of viscosity and Young's modulus of materials under test. For calibration purposes of the developed setup, glycerin/water mixtures and methylcellulose/water solutions were characterized as viscous and polyacrylamide gels as elastic materials, respectively. In addition, the interfacial tensions were calculated with respect to the magnetic Bond number from the droplet deformations. For the first time, the transient rheological behavior of viscoelastic material was measured using the method of ferrofluid droplet deformation. When polyacrylamide gel with a shear modulus of 230 Pa was evacuated for less than 40 min during preparation, it showed a strong time-depending viscoelastic behavior several minutes after starting the measurements. Here, Young's modulus increased up to the value of elastic behavior, whereas the values for viscosity decreased to a baseline. The developed setup can favorably be used in future applications to investigate local and also time-dependent rheological properties of soft materials.

1. Introduction

The characterization of elastic, viscous, and viscoelastic properties of soft materials is of permanent interest. When the shear modulus of the material under investigation depends on time or frequency, the material shows viscoelastic properties, which means that the material exhibits a viscous and an elastic response. Measurements of bulk viscoelastic properties of macroscopic samples are usually performed with mechanical rheometers by deforming the whole material at varying frequencies up to tens of Hertz [1].

To provide insight into viscoelastic properties on the micrometer scale, magnetic setups have been developed, in which a chemically inert magnetic bead is inserted into the material under test (MUT) and displaced by externally applied magnetic forces. In combination with modern high-resolution microscopy and video analysis, the active manipulation of the probes makes the characterization of local viscoelastic properties feasible. Freundlich and Seifriz pioneered this technique of active manipulation of magnetic microbeads in the nineteen-twenties [2]. In such magnetic tweezers setups, magnetic forces can be generated either by permanent magnets or electromagnets, whereas electromagnets are preferred due to the easy control of magnetic forces by adjusting the coil currents. The output forces can be strengthened by using soft magnetic cores with high saturation magnetization. Magnetic tweezers exert a force on the beads generated by a magnetic field gradient that can be controlled using different magnet assemblies. In solenoid tweezers, a coil is wound around a cylindrical soft magnetic

* Corresponding author.
E-mail address: schnakenberg@iwe1.rwth-aachen.de (U. Schnakenberg).

https://doi.org/10.1016/j.sna.2022.113756
Received 7 April 2022; Received in revised form 23 June 2022; Accepted 11 July 2022
Available online 16 July 2022

core that is tapered to a tip at one end, e.g., by electropolishing [3–5]. Unfortunately, electropolishing is an isotropic etching process and leads to low accuracy and reproducibility of the tip geometry [6]. To increase the reproducibility and place accuracy in tip manufacturing, planar magnetic tip arrangements have been developed with microsystem technologies, like photolithography and electroplating. These technologies allow for the most accurately produced microstructures. In comparison, easy to handle laser cutting of magnetic films results in slightly more imprecise structures and suffers from oxidation phenomena at the cutting edges [7]. Besides two-pole arrangements [8,9], arrangements with three [10,11] or four poles [12,13] for two-dimensional manipulation and even six poles [14] for three-dimensional bead manipulation have been reported.

An inherent problem of such magnetic tip-based designs is the poor control of force due to the highly nonlinear force-distance relationship caused by the required inhomogeneous magnetic field gradient. In multipole arrangements, a homogeneous field gradient and therefore a constant force can be generated only within small areas [11–13]. Nevertheless, the force can be increased by arranging the tips closer [11].

To prevent these serious disadvantages, ferrofluid droplets in combination with homogeneous magnetic fields can be used. A ferrofluid consists of superparamagnetic surfactant-coated nanoparticles suspended in an oil or water-based solution. When a homogeneous magnetic field is applied, the magnetic moments of the particles orient along the field and generate magnetic stress. This principle can favorably be used for actuators, e.g., for the manipulation of droplets [15–20], seals [21], valves, pumps, stepping motors [22–27], optical switches [28], generating pressure [29] as well as for sensors, e.g., measuring tilt [30,31], flow [32], and magnetic field [33], respectively. Furthermore, Yang et al. published an excellent review on micro-magnetofluidics in microfluidic systems [34].

To characterize viscoelastic properties on a micro-scale, ferrofluid droplets can be injected into the MUT with the help of a micropipette. The ferrofluid droplet deforms axisymmetrically into a prolate spheroid along the direction of the magnetic field [35,36]. By video recording, the droplet deformation dynamics upon actuation can be calculated. By time-resolved measurement of minor and major ellipse radii, the creep response curves exhibit an elastic domain, a relaxation regime, and a viscous flow behavior. In addition to the analytical descriptions [35–37], this response can be simulated by an application-adapted mechanical equivalent circuit consisting of springs and dashpots [38,39]. The ferrofluid droplet approach is a non-destructive technique compared to the magnetic bead approach, where the bead destroys the surrounding biological MUT during its displacement. Therefore, measurements with ferrofluid droplets can be carried out several times to investigate changing rheological properties of the MUT.

Pioneered work was carried out by Serwane et al. [38]. They quantified micro-scaled viscoelastic properties in living embryonic tissues by using ferrofluid droplets and eight magnets in a Halbach configuration to obtain homogeneous magnetic fields in different directions. In our work, we simplify Serwane's idea and propose a magnetic setup in the Helmholtz arrangement, which consists of two circular wire coils oriented parallel and coaxial to each other. The setup is calibrated with viscous and elastic MUTs. For the first time, transient viscoelastic behavior is measured with the method of ferrofluid droplet deformation. Polyacrylamide (PAAm) gels show viscoelastic behavior depending on the evacuation time during preparation. The experimental results are described analytically and with mechanical equivalent circuits consisting of springs and dashpots.

2. Theory

For the sake of completeness, the theoretical background is recapped here and adopted for the case of ferrofluid droplet deformations in MUTs. Pure viscous or elastic materials can be represented by a simple dashpot or spring element, respectively. Dashpots, in general, represent viscosities η, whereas spring elements E represent elastic (Young's) moduli. In our system, the impact of interaction between the ferrofluid droplet and the surrounding MUT must always be considered. The applied magnetic field strength deforms the ferrofluid droplet, which in turn deforms the surrounding material. Since the magnetic field is homogenous, the ferrofluid droplet elongates axisymmetrically in an ellipsoidal shape. The magnetic stress σ_M can be calculated to $\sigma_M = \mu_0 M^2/2$, with $\mu_0 = 4\pi * 10^{-7}$ N/m representing the magnetic permeability in free space and M the magnetization of the ferrofluid, respectively [38]. For small droplet deformations, the 3D problem of the ferrofluid droplet actuation in a MUT can be reduced to a 1D description of the uniaxial strain and stress along the direction defined by the magnetic field [38]. The deformation is limited by the capillary stress caused by interface tension between ferrofluid and MUT [35–38]. For small deformations, the capillary stress can be represented by a Hooke spring E_0 [38]. This spring E_0 depends on the droplet size. For viscous MUTs, E_0 acts in parallel with the dashpot (Fig. 1**a**) to take the recovery of the droplet to its initial shape after switching off the applied stress into account. In the case of an elastic MUT, the spring E_0 is also connected in parallel to E_1, as shown in Fig. 1**b**. Spring element E_0 is referred to "elastic input of the ferrofluid" throughout the manuscript. It has to be noted that the viscosity of the ferrofluid of 80 mPa*s can be neglected with regard to all MUTs investigated here.

For the calibration of the setup, viscous and elastic reference MUTs were investigated. For both cases, viscosity, respective elasticity, in combination with the ferrofluid droplet actuation, can be described as depicted in Fig. 1**a** and **b**. In general, dashpot η and spring elements E can be expressed by [1,39].

$$\sigma = \eta \bullet \dot{\varepsilon} \tag{1}$$

$$\sigma = E \bullet \varepsilon \tag{2}$$

with $\dot{\varepsilon} = \frac{d\varepsilon}{dt}$, $\sigma = \sigma_M$ represents the applied magnetic stress and ε the strain, respectively. Since we do not have any other additional stress, the index M in the magnetic stress symbol σ_M can be neglected. Applying Eqs. (1) and (2) to Fig. 1**a**, we obtain a differential equation

$$\sigma = \quad \eta\dot{\varepsilon} + E_0\varepsilon \tag{3}$$

The solution of this equation describes the so-called creep regime in which the stress is constant and the strain is the time-dependent variable

$$\varepsilon(t) = \frac{\sigma}{E_0}\left(1 - e^{\frac{-(t-t_0)E_0}{\eta}}\right) \tag{3a}$$

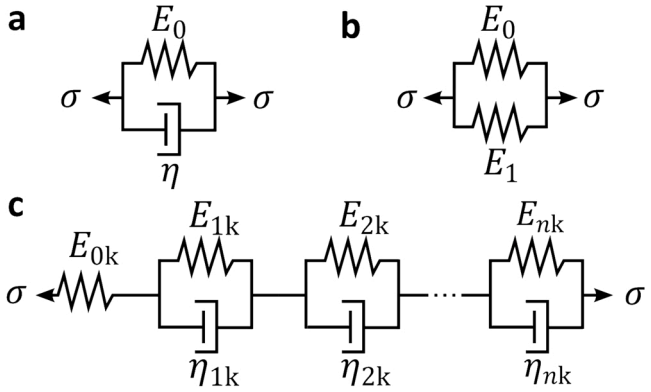

Fig. 1. Scheme of theoretical models for a ferrofluid droplet in MUT: (a) Viscous MUT with viscosity η represented by a dashpot. (b) Elastic material is represented by a spring E_1. In both figures, the capillary stress of the ferrofluid droplet is given by a Hooke spring E_0 connected in parallel. (c) Generalized Kelvin-Voigt model for describing the creep behavior of viscoelastic solids under constant applied stress with more than one relaxation time.

Here, t_0 represents the time point at which the magnetic field is switched on.

On the other hand, by applying Eq. (2) to Fig. 1**b**, we obtain Hooke's law for a continuous material in one dimension

$$\sigma = (E_1 + E_0)\varepsilon = E_A\varepsilon \tag{4}$$

Here, $E_A = E_0 + E_1$ is the apparent elasticity, spring E_0 the elastic input of the ferrofluid droplet and spring E_1 the elastic (Young's) modulus of the elastic material, respectively.

Maxwell and Kelvin-Voigt models are used to describe viscoelastic material behavior, [36]. Viscoelastic solids, as in our case, can be described by the generalized Kelvin-Voigt (GKV) model, whereas for viscoelastic liquids, the generalized Maxwell model (GM) are typically used [38]. The GKV model describes creep behavior while the GM model is better to describe stress relaxation phenomena [39]. Therefore, the GKV model for describing viscoelastic behavior is used in this work.

A viscoelastic solid in combination with a ferrofluid droplet can be described by the generalized Kelvin-Voigt (GKV), as shown in Fig. 1**c**. The GKV model is a series of Kelvin-Voigt elements with a spring, all of them connected in series. The spring element E_{0_k} represents the elastic input of the ferrofluid droplet and each KV element its own viscoelastic contribution to the whole system, respectively. By reconfiguring the GM model description of Serwane et al. [38] for the GKV model case here, the creep regime of the generalized KV model can be expressed with respect to the creep compliance $J(t) = \varepsilon(t)/\sigma$ [39].

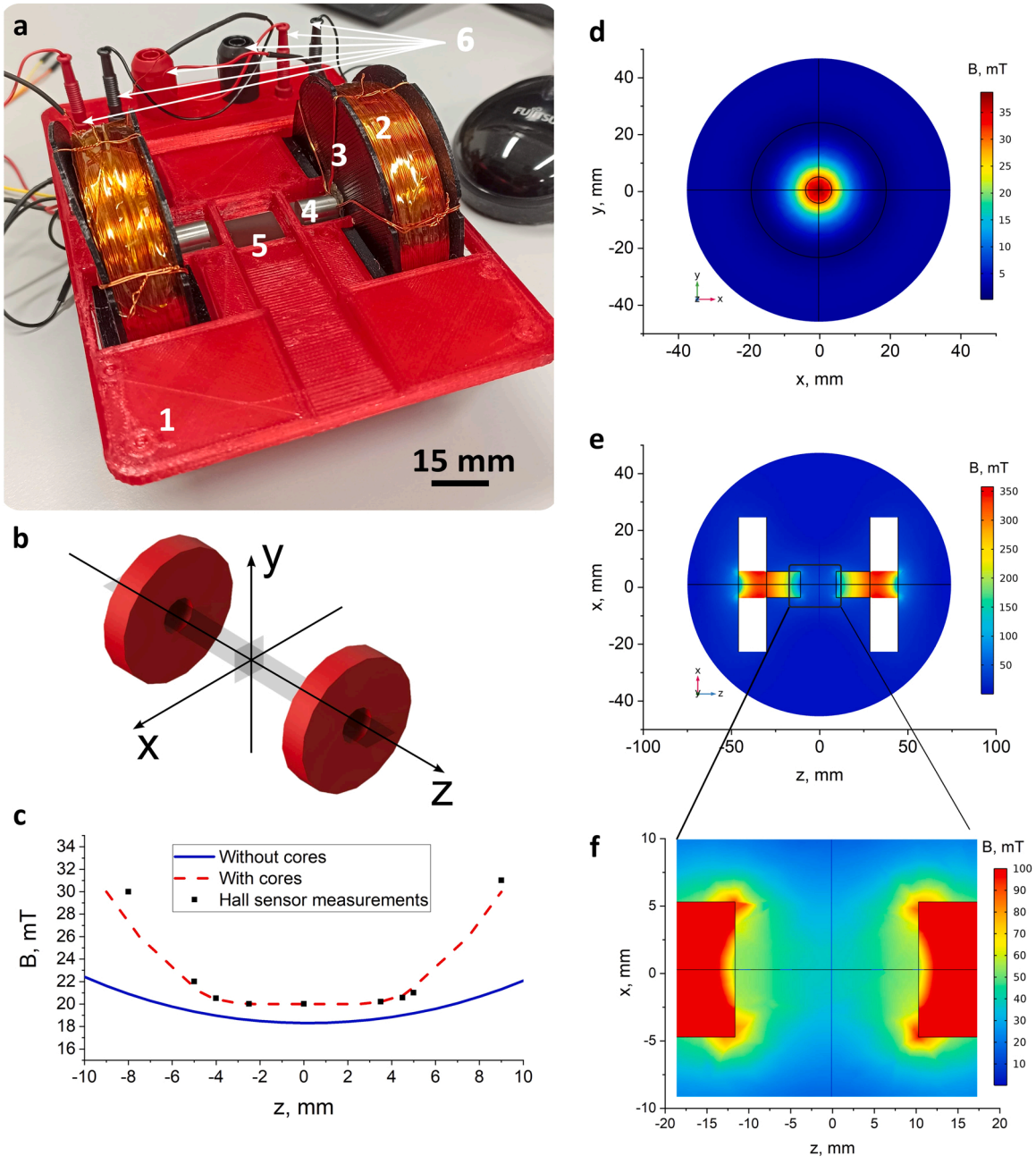

Fig. 2. Magnetic setup. (a) Photo of the magnetic setup. The numbers represent different parts of the setup: 1 - baseplate, 2 - copper coil, 3 - plastic coil case, 4 - metal core, 5 - recess for coverslip with MUT (18 ×18 mm), 6 - plugs and sockets for power supply connection. (b) Sketch of the magnetic setup geometry. The origin of the coordinate system corresponds to the center point between two coils. (c) Magnetic field *M* distribution along the z-axis around the zero point in the absence and presence of cores. (d)-(f) FEM simulations of magnetic field distribution in *z*/*x* (e) and *x*/*y* (f) planes by application of 1 A current to each coil with cores.

$$\varepsilon(t) = \sigma \frac{1}{E_{0_k}} \left[1 + \sum_{i=1}^{n} \frac{E_{0_k}}{E_{ik}} \left(1 - e^{-\frac{t}{\tau_{ik}}} \right) \right] \tag{5}$$

where $\tau_{i_k} = \eta_{i_k}/E_{i_k}$ represents the recovery time, E_{i_k} and η_{i_k} the elastic and viscous contribution of the ith component in the GKV model, respectively.

It should be noticed that the values of elastic elements in the GKV model (Fig. 1**c**) are not the same as spring elements in the linear elastic model (Fig. 1**b**). However, all springs can be subsumed under one spring which represents apparent elasticity E_A. Then, the relation between apparent E_A elasticity and spring elements in Fig. 1**b** and Fig. 1**c** can be written as

$$\frac{1}{E_1 + E_0} = \frac{1}{E_A} = \sum_{i=0}^{n} \frac{1}{E_{ik}} \tag{6}$$

3. Experimental and results

3.1. Magnetization of ferrofluid

The magnetization of the ferrofluid was determined with a PPMS-DynaCool magnetometer (Quantum Design) with the vibrating sample magnetometry (VSM) option. Approximately 1 mg of ferrofluid was filled into a powder capsule pair. Fig. A1a shows the linear and non-linear parts of the magnetization with respect to applied magnetic field strength. The non-linear part was fitted by a logarithmic function $y(x) = 4250\ln(x) - 28100$, while the linear part was fitted by a function $y(x) = 1.5x + 650$, according to Afkhami et al. [35]. In addition, a Langevin fit is shown. In Fig. A.1b, the magnetic susceptibilities of ferrofluid $\chi = \mathrm{d}M/\mathrm{d}H$ with respect to magnetic field strength H, whereas in Fig. A.1c, the dependency of the magnetic stresses σ on magnetic field strength H with respect to different magnetization M(H) for the measurement and fitting curves are depicted, respectively.

3.2. Setup

The magnetic setup is based on a Helmholtz arrangement with two electromagnets. The coils are positioned coaxially by a fixture whose coil cases and the baseplate were 3D-printed (Anycubic Mega X 3d printer) using PET-G plastic filament (Geeetech), as shown in Fig. 2**a** and 2**b**. One coil itself has an inner diameter of 14 mm, an outer diameter of 72 mm, and a width of 15 mm, respectively. Each coil has an electrical resistance of 77 Ω obtained with 3000 turns of a copper wire with 0.3 mm in diameter. Martensitic steel cores (Steel EN 1.4021 (AISI 420), Rosen Metal Service GmbH) are added to the coils. The two coils are electrically connected in parallel. The currents through the coils were measured by current sensors (INA219, Adafruit Industries LLC) and were controlled by a Raspberry Pi 4.

FEM simulations were carried out in COMSOL Multiphysics® to specify the magnetic field between the coils (Fig. 2 **c-f**). The magnetic field distribution along the z-axis was simulated without cores according to [40] and compared with metal cores (Fig. 2**c**). The simulations were confirmed by magnetic field measurements using a Hall sensor (GaAs Hall Element CYSJ902, Sonnecy). According to the simulations, a maximum magnetic field of 18 mT can be generated by applying 100 W power (1 A, 100 V) to the coils and can preferably be increased by a factor of 1.3 with a reduction of the magnetic field gradient by adding 33 mm long cores to both coils. FEM simulations of the magnetic field distribution in zx- and xy- planes (Fig. 2**e** and **f**) allow us to allocate a central cylinder-shaped magnetic field volume of 5 mm radius and 5 mm side length, in which the magnetic field changes only within 1 %.

The setup can be used either with an upright or inverse microscope since the distance between the coils was adjusted to 55 mm. For our experiments, the inverted microscope Olympus IX70 with Olympus UPlanFL N 4X or 20X objective with nonmagnetic aluminum shielding was used. Video recordings were taken with a standard HD Raspberry Pi camera (12.3 megapixel Sony IMX477 sensor) that was connected to the microscope with a custom-made 3D printed adapter.

An Eppendorf manipulator was utilized to place the injection capillary precisely into the MUT. The capillary was made from a borosilicate glass with the help of a laser-based micropipette puller (P-2000, Sutter Instrument). The inner diameter of the capillary tip was determined to be around 50 μm. In addition, commercially tailed capillaries (ICSI Pipettes - Blunt, BioMedical Instruments) with a tip inner opening diameter of 5 μm were used (Fig. A.2). With regard to the droplet injection procedure, capillary effects, ferrofluid adhesion to the glass capillary in viscosity tests as well as MUT stickiness to the capillary in elasticity tests were prevented by coating the capillary tips prior to the droplet injection. For the hydrophilic PAAm gels, the capillary tips were dipped in a hydrophobic reagent (26014 Regenabweiser, Rain-X) [41]. On the other hand, the viscous MUTs, especially those with low viscosities, exhibit insufficient friction forces that could strip the droplet from the yanking capillary. In these cases, the surface of the glass capillary was made oleophobic (hydrophilic) by dipping the capillary tip in BSA solution [42]. In both cases, the capillaries were dipped for 5 min and then dried at room temperature.

For the experiments, the magnetic field was periodically switched on and off. The minor and major droplet radii a and b were measured during ellipsoid forming, see Fig. A.2.

3.3. Reference measurements on viscous MUTs

As references for pure viscous MUTs, two glycerin/water (2036, Th. Geyer) and methylcellulose/water (Methylcellulose 4000, Sigma Aldrich) solutions were used. 2 % (w/v) methylcellulose solution was prepared according to the procedure briefly summarized in the appendix section Supplementary Data. Ferrofluid droplets (MFR-DP1, MagronCo., Ltd) with radii of 20–150 μm were injected into 30 μL droplets of the MUTs. For 99.95 % (v/v) glycerin, the droplets were injected into the purchased MUT, whereas for the 99.35 % (v/v) glycerin, the droplets were injected directly after the preparation to minimize moisture uptake. The magnetic field was periodically switched on and off at least three times for 15 s (Fig. A.3). For example, the b/a ratios were plotted over time for 99.95 % (v/v) glycerin, as depicted in Fig. A.3. From these curves, the average strain $\varepsilon = 2(b/a - 1)/3$ values were calculated and plotted over time (Fig. 3**a**), according to [38].

For fitting purposes, the Wolfram Mathematica software was used to obtain values for the viscosities η of the MUTs and the elastic contribution E_0 of the ferrofluid droplet from Eq. (3a). By comparing the calculated values for glycerin/water viscosities with the reference values η_{ref} given by [43], while for methylcellulose, the value was taken from the datasheet, a calibration factor of 125 was obtained. In Fig. 3**b**, the calculated viscosity values from measurements multiplied by the reciprocal of the calibration factor are plotted with respect to the reference values of the viscosities of the three viscous MUTs. As expected, the reference curve is a straight line.

As mentioned above, the elastic contribution E_0 of the ferrofluid droplet depends on the droplet size and can be expressed in the form of [38].

$$E_0 = \frac{k \bullet \gamma}{R} \tag{7}$$

where γ is the interfacial tension and k the proportionality coefficient, respectively.

After taking E_0 from the fitted curves of creep data (Fig. 3**a** for different droplet sizes), E_0 is plotted with respect to $1/R$, as shown in Fig. 3**c**. The calculated values of the slopes $k \bullet \gamma$ for the three characterized MUTs are summarized in Table 1.

The interfacial tensions γ of all characterized MUTs can be determined from the magnetic Bond number Bo_m [44].

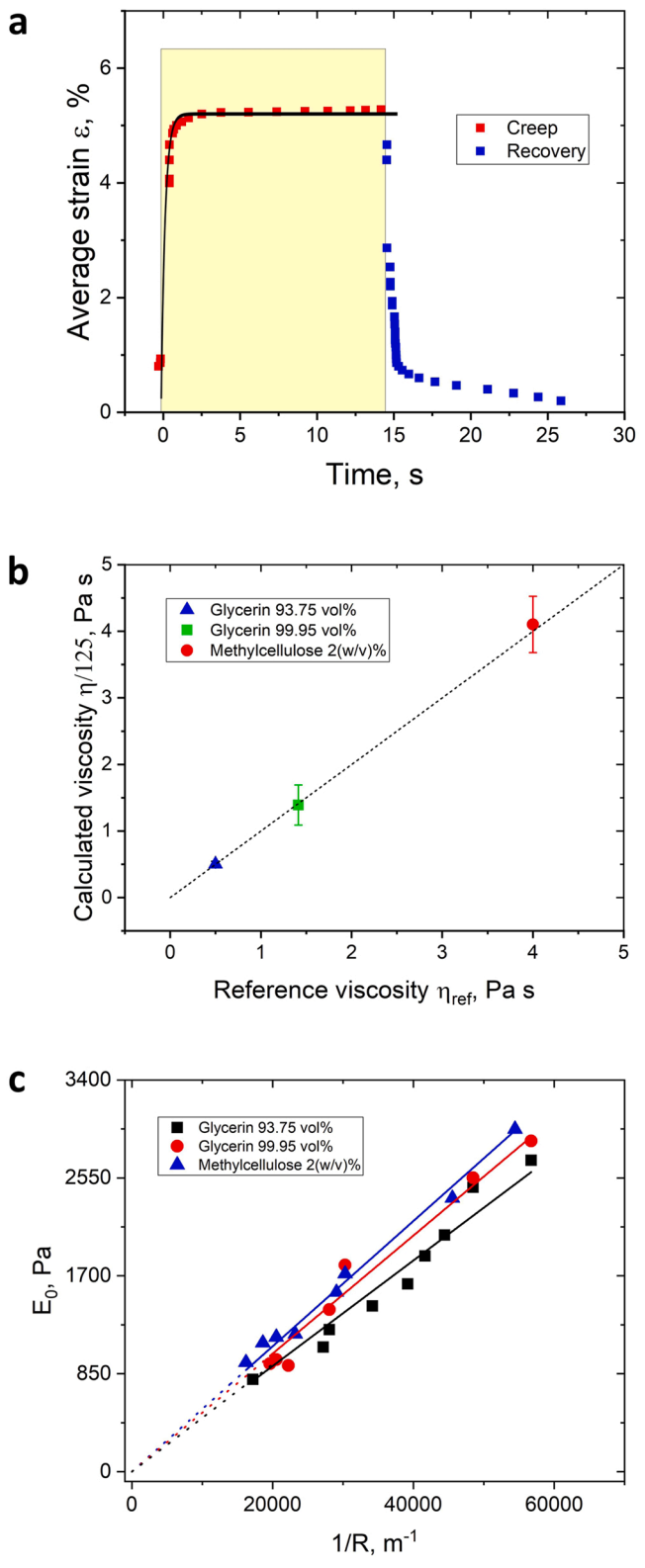

Fig. 3. Ferrofluid droplet deformation in 99.95 % (v/v) glycerin: (a) Calculated average strain with respect to time. Black solid line shows the fitted curve according Eq. (3a). The yellow rectangle shows the period of the applied magnetic field (20mT). (b) Calculated viscosities from measurements multiplied with the reciprocal of the calibration factor with respect to the reference viscosities for three viscous MUTs. The reference line is depicted. Error bars indicate standard deviation. (c) Dependency of the elastic contribution of the ferrofluid droplet E_0 on the reciprocal droplet size R. Fitting data are summarized in Table 1.

Table 1
Calculated interfacial tension γ, slopes $k \bullet \gamma$ and coefficient of correlation R_s^2 for the three characterized viscous MUTs.

	γ, N/m from Eq. (8)	$k \bullet \gamma$, N/m extracted from slopes in Fig. 3c	R_s^2
Glycerin 93.75 % (v/v)	0.0028	$0.04 \pm 2.6 \bullet 10^{-3}$	0.99068
Glycerin 99.95 % (v/v)	0.0032	$0.045 \pm 1.9 \bullet 10^{-3}$	0.99457
Methylcellulose 2 % (w/v)	0.0039	$0.054 \pm 1.3 \bullet 10^{-3}$	0.99844

$$Bo_m = \frac{R\mu_0 H^2}{2\gamma} \tag{8}$$

The magnetic Bond number is the ratio of magnetic force to interfacial tension force. Afkhami et al. showed in their model that the magnetic Bond number Bo_m is related to the droplet elongation, represented by the b/a ratio [35]:

$$Bo_m = \left(\frac{1}{\chi_{sys}} + k_d\right)^2 \left(\frac{b}{a}\right)^{\frac{1}{3}} \left(\frac{2b}{a} - \left(\frac{b}{a}\right)^{-2} - 1\right) \tag{9}$$

The system susceptibility $\chi_{sys} = (\mu_d - \mu_m)/\mu_m$ depends on relative magnetic permeabilities of ferrofluid μ_d and MUT μ_m. In case of non-magnetic MUTs ($\mu_m = 1$), the system susceptibility equals the susceptibility of the ferrofluid $\chi_{sys} = \chi$ (Fig A1b). The demagnetization factor k_d is given by [35,44]:

$$k_d = \left(\frac{(1 - Ec^2)}{2Ec^3}\right)\left(\ln\left(\frac{1 + Ec}{1 - Ec}\right) - 2Ec\right) \tag{10}$$

Ec is the eccentricity of the droplet and is expressed by:

$$Ec = \sqrt{1 - \frac{a^2}{b^2}} \tag{11}$$

For each MUT, the magnetic Bond number Bo_m was calculated according to Eqs. (9) - (11) based on the measured radii a and b values of the deformed droplets. The calculated interfacial tensions of the three MUTs from Eq. (8) are summarized in Table 1.

By considering the slope values from Fig. 3**c**, we obtained a k-value of 12.8 for all three MUTs, according to Eq. (7).

3.4. Reference measurements on elastic PAAm gels

To calibrate our setup for elastic materials, weakly cross-linked PAAm hydrogels were chosen. The preparation of PAAm gels with shear moduli G of 230 Pa, 689 Pa and 1535 Pa was carried out according to [45] and is briefly summarized in the appendix section Supplementary Data. The working solutions of 1 mL were prepared from a stock solution of 5 mL (see Table A.1).

In 7 min after placing the gel on a glass slide, ferrofluid droplets of different initial radii R were injected in PAAm gel samples. To prevent leakage of ferrofluid, the capillary was slowly extracted from the gel. Since gels were weakly cross-linked and the capillary outer diameter was small, the channel was tightly closed by internal stress relaxation. The b/a-values over time were recorded under a continuously changing magnetic field (Fig. 4**a**). The magnetic stress $\sigma = \mu_0 M^2/2$ was calculated in the logarithmic and in the linear regime, according to Fig. A.1. We obtained stress-strain diagrams, as exemplarily depicted in Fig. 4**b**, for a PAAm gel with a shear modulus G of 689 Pa. With respect to Eq. (4), we calculated the values of the apparent elasticities E_A from the slopes of the fitting curve. Fig. 4**c** shows the apparent elasticities E_A of the three PAAm gels with respect to reciprocal initial droplet radius R. Since $E_A = E_1 + E_0 = E_1 + \frac{k \bullet \gamma}{R}$, we obtain a linear dependency for all characterized PAAm gels, as shown in Fig. 4**c**.

The relation between elastic (Young's) modulus E and shear modulus

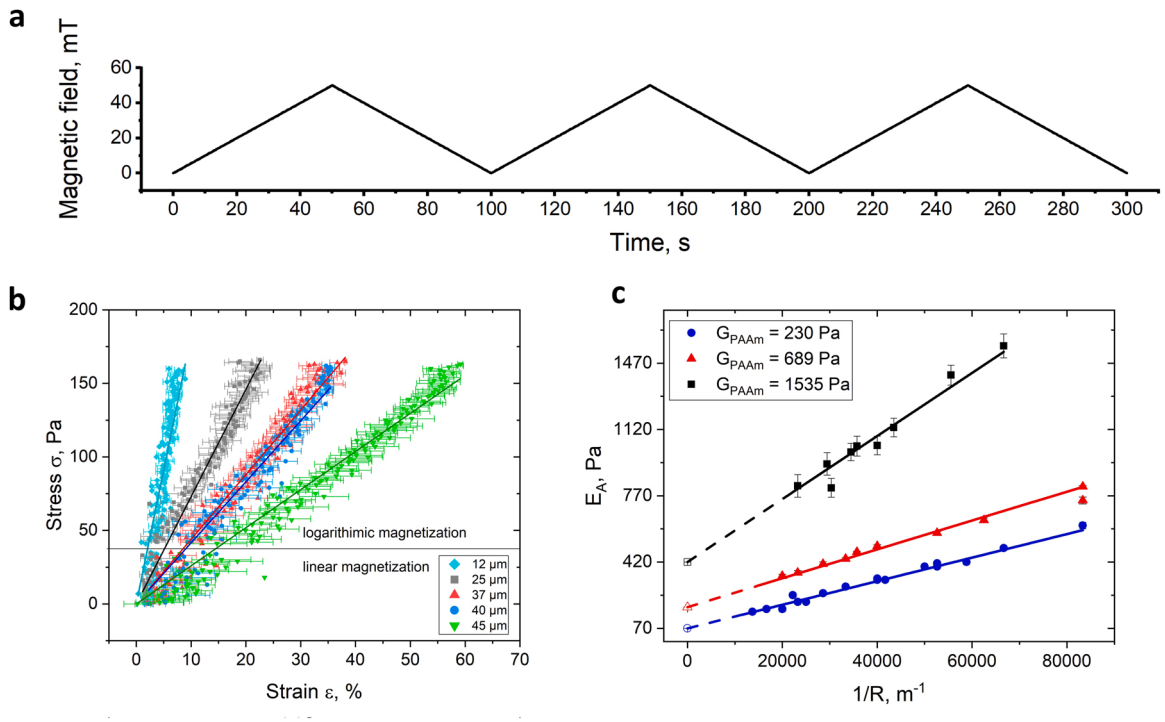

Fig. 4. (a) Changing magnetic field in continuous mode. (b) Stress-strain diagrams of different ferrofluid droplet sizes in a PAAm gel with a shear modulus of 689 Pa. Stress was calculated separately for the linear and logarithmic magnetization region. (c) Apparent elasticity E_A of the PAAm gels with respect to reciprocal of droplet radius R of undeformed droplets. Hollow points show extrapolation to $R = \infty$. Error bars represent standard deviation.

G can be expressed in form of

$$E = 2G(1+\nu) = 3G \tag{12}$$

for a Poisson's ratio ν of 0.5 for rubber-like polymers as gels [45,46].

The values for Young's moduli E of the different gels can be easily determined as $E_1 = E/10$ by the intercepts of the ordinate axis and comparison to reference values. The fitting parameters of the curves are summarized in Table A.2 and Table A.3.

Table 2 summarizes the shear moduli G, the calculated (with reference to Eq. (12)) as well as the extracted Young's moduli E from measurements of the PAAm gels, respectively. For all characterized PAAm gels, the calculated and extracted Young's modulus correspond to around 3%.3 %.

3.5. Characterization of viscoelastic behavior on PAAm gels

In contrast to the elastic behavior of PAAm gels described in chapter 3.3, the PAAm gel with a shear modulus G of 230 Pa showed a strong time-depending viscoelastic behavior during the first minutes of measurements depending on the preparation. To investigate this phenomenon in detail, the working solution was prepared as described. The final solution of 6.3 mL was divided into equal parts and transferred into 21 Eppendorf safe-lock tubes. Before gelation, the ensemble was divided into 7 groups, with 3 tubes in each group. The tubes of the first group were closed without any additional external influence, while, in contrast, all other groups were evacuated a second time for different periods (from 10 min to 60 min in 10-minute steps) and then closed for gelation. Measurements with ferrofluid droplets were carried out the day after. One minute after the gel was taken from the tube and put on a coverslip, the ferrofluid droplet was injected, and a constant magnetic stress σ of 40 Pa was applied periodically. As before, the b/a-ratios were measured and the strain values ε were calculated. In Fig. A.4, strain values are plotted over time for the first four periods of the applied magnetic field. Eq. (5) with $n = 1$, which describes the viscoelastic behavior of homogenous and isotropic materials, was fitted to every creep curve and values for elastic E_{1_k}, E_{0_k} and viscous η_{1k} elements were obtained. Apparent elasticity E_A was calculated according to Eq. (6). The elastic input of ferrofluid droplet E_0 was obtained from Eqs. (7) to (11). Then, Young's modulus E was calculated as the difference of E_A and E_0. The dashpot η_{1k} is equal to the dashpot η as shown in Fig. 1**a**, so that the values represent the values of viscosity**.** Results are depicted in Fig. 5. For evacuation times below 40 min, Young's moduli increased within 400 s until reaching the value for pure elasticity (see Table 2), whereas the values for viscosity decreased to a baseline. In comparison, for evacuation times of 40 min and above Young's modulus as well as the viscosity do not change with time and show both the value of pure elasticity and of the baseline, respectively.

Table 2
Shear modulus G, calculated and extracted Young's moduli E.

Shear modulus G, Pa	Calculated Young's modulus $E = 3G$, Pa	Extracted Young's modulus E, Pa	Error between calculated and extracted Young's moduli
230	690	701 ± 68	1.6 %
689	2067	2030 ± 129.5	1.8 %
1535	4605	4753 ± 225	3.2 %

4. Discussion

The characterization of viscoelastic properties of soft materials is always of high interest. Besides macroscopic measurement devices, such as rheometers, miniaturized devices for measuring localized viscoelastic properties were developed, typically using magnetic microbeads, which are displaced in the MUT by applying a gradient magnetic field. These fields are often generated by a solenoid type electromagnet, which is placed in the immediate neighborhood of the microbeads. On the other hand, Serwane et al. showed for the first time impressively that local viscoelastic properties can be determined by applying a homogeneous magnetic field to a ferrofluid droplet, which forms an ellipsoid in soft

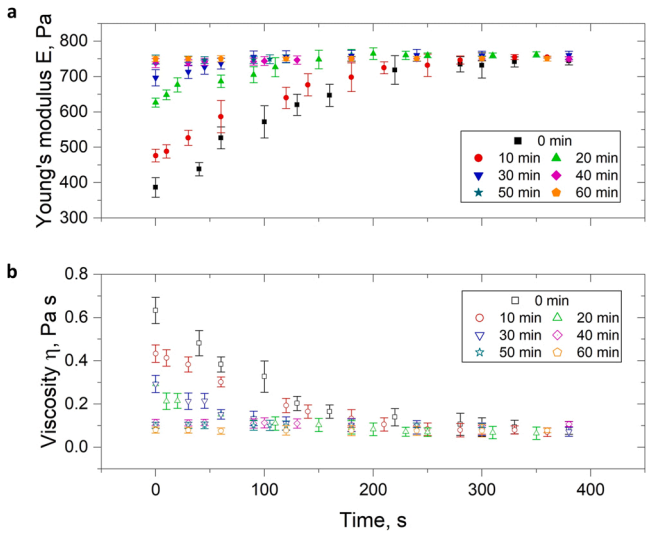

Fig. 5. Time dependency of Young's modulus (a) and viscosity (b) of PAAm gels with a shear modulus of 230 Pa. The gels were prepared with different evacuation times before gelation in closed Eppendorf safe-lock tubes. Error bars represent standard deviation.

materials [38]. However, they used a complex magnet arrangement in the Halbach configuration, because the interest was in measuring anisotropic viscoelastic material properties. To generate homogeneous magnetic fields in any horizontal direction, each of the eight circular arranged magnets was aligned individually by servomotors.

Nevertheless, characterizations of isotropic materials allow the use of simplified magnet arrangements. In contrast to Serwane's group, we developed a magnetic setup in Helmholtz arrangement using two parallel-arranged coaxial coils. Our setup was simple to manufacture utilizing low-cost state-of-the-art 3D-printing technologies (see Fig. 2). The generation of the magnetic field was carried out by a tunable power supply, which was connected to the coils. In our setup, the distance between the two electromagnets coils was adjusted to fit an inverted or upright microscope by replacing the microscope's universal holder (size 160 mm × 110 mm). FEM simulations and measurements (see Fig. 2 **d-f**) have shown that a homogeneous magnetic field over a cross-section of 10 mm in diameter was obtained with the defined coil arrangement, which determines the maximum size of the MUTs. Using our coil arrangement with added cores, a maximum magnetic field of around 44 mT can be achieved. In combination with a saturation magnetization up to 20 kA/m of the used ferrofluid, Young's moduli not larger than several kPa can be determined. Utilizing our setup for future applications, the measurement of anisotropic material behavior can easily be carried out by rotating the MUT in the magnetic field.

The time constant τ for switching on and off the magnetic field can be calculated to 3 ms according $\tau = L/R_{coil}$, where L is the inductance and R_{coil} is the electrical resistance of the coil. This time constant is much lower than the measured time constant τ_m (time between 10 % and 90 % of the rising b/a ratio) of 33 ms obtained from the data shown in Fig. A.3. Therefore, it can be stated that a constant magnetic field without significant delay is applied to the ferrofluid droplet.

The magnetization of the ferrofluid was measured with a magnetometer and showed a linear behavior between 0 kA/M and 5 kA/m of the applied magnetic field strength and a logarithmic behavior above (Fig. A1), which was also observed by Afkhami et al. [35] and Serwane et al. [38]. In addition, the magnetization data was also fitted with a Langevin function [47]. In comparison, the logarithmic function shows a better fit to the experimental data in the magnetic field range between 5 and 50 kA/m, as also pointed out by Afkhami et al. [35]. The deviation of the Langevin function from the experimental data in the same range can be explained by particle-size distribution within the ferrofluid probe. Since the magnetization exhibit a nonlinear behavior, the magnetic susceptibility of ferrofluid $\chi = dM/dH$ was calculated and depicted in Fig. A.1b. Also we considered the dependency of magnetic stresses $\sigma = \mu_0 M(H)^2/2$ on magnetic field strength H with respect to different magnetization $M(H)$ for the measurement and fitting curves (Fig. A1c). There the Langevin function fitting again shows deviation in the range used. Therefore, the piecewise function which consist of linear and logarithmic fits was chosen as best approximation of experimental data.

Viscous or elastic materials can be described by a dashpot or spring indicating elastic and viscous inputs, respectively. In comparison to other measurement techniques, the contribution of the ferrofluid droplet has to be considered. The capillary stress of the droplet limits its deformation by the magnetic field. This capillary stress can be approximated by a Hooke's spring E_0 for small deformations, which is placed in parallel to the dashpot for viscous MUTs, or the spring, for elastic MUTs, as depicted in Fig. 1.

Viscous glycerin/water mixtures are often used as reference materials. To enlarge the measurement range, 2 % (w/v) methylcellulose was chosen in addition. After monitoring the b/a ratio of the deformed droplet under the applied homogeneous magnetic field (Fig. 3), the time-dependent average strain was calculated, from which the calibration factor of 125 between the measured and reference viscosity values was determined within an error below 5 % (Fig. 3**b**).

Since the densities of ferrofluid and viscous MUTs are different, ferrofluid droplets slowly float up after injection. Measurements were carried out during droplet floating in the MUT until it touched the top MUT surface and collapsed. The last several measurements were not considered. In general, the drift of ferrofluid droplets during measurements was also reported by Serwane et al. [38]. We assume that the lifting has no significant influence on our measurements, because the magnetic field was applied for only short periods. In addition, no leakage of ferrofluid during droplet deformation was observed at the puncture site.

The elastic input E_0 of the ferrofluid was determined from the measurements in pure viscous MUTs. Our results confirm the observation of Serwane et al. that E_0 depends linearly on the reciprocal of the droplet size [38]. With reference to the magnetic Bond number Bo_m [35, 44], the interfacial tension can easily be determined for the different MUTs. The determination of the interfacial tension of a ferrofluid droplet in a MUT by measuring the minor and major ellipsoid radii during droplet deformation is a decisive advantage of the method.

In comparison to viscous MUTs, the elastic PAAm gels were measured by the application of continually changing magnetic fields (Fig. 4**a**). Linear stress-strain diagrams (Fig. 4**b**) confirm that the PAAm gels behaved elastically, as expected [38]. The slopes of the fitting curves in Fig. 4**b** depend on droplet sizes. As proposed by [38], by plotting the apparent elasticity E_A with respect to $1/R$ (Fig. 4**c**), Young's modulus E of all three characterized PAAm gels can be determined by the intercepts of the linear fitting curves at the ordinate. The obtained Young's modulus values agree well within around 3 % to the reference values (Table 2).

To the best knowledge of the authors, measurements of transient rheological properties by using ferrofluid droplet deformation method were not reported so far. For a proof-of-concept, PAAm gels with a shear modulus of 230 were characterized. They exhibit generally elastic behavior but show a strong time-depending viscoelastic behavior within the first 400 s after starting the measurements as a function of the evacuation time of the gel solution prior to pouring the gel. As shown in Fig. 5 for evacuation times below 40 min, Young's moduli increased to the value of elasticity, whereas the viscosities decreased until reaching a baseline. The formation of PAAm hydrogels proceeds due to free radical polymerization. It is well known that oxygen serves as a free radical trap by generating dead chain ends [48]. Oxygen, as an inhibitor of polymerization, is present in the gel solution prior to pouring. One of the most critical steps in the preparation of PAAm gels is the evacuation, or

"degassing", of gel solutions prior to pouring the gel [48–50]. Proper evacuation of the PAAm solution leads to the reduction of the oxygen content and a higher degree of polymerization. It is worthwhile to mention that the PAAm gels were polymerized in closed Eppendorf self-lock tubes, in which a balanced atmosphere during gelation was established. Fig. 5 indicates that after opening the Epi-tube for measurements, the polymerization process continued within 400 s for PAAm gels which were evacuated below 40 min. In comparison, for those PAAm gels, which were evacuated for more than 40 min, most of the oxygen is extracted during the evacuation, and the remaining oxygen content in the gels seemed to be low compared to the concentrations of monomer and cross-linker so that the oxygen is consumed evenly during the polymerization reaction [48]. These gels and also non-evacuated gels with a shear modulus of 1535 Pa showed pure elastic behavior with constant values of Young's modulus and viscosities for all times (see Fig. 5). For completeness, however, it should be noted that the non-evacuated PAAm gel with shear modulus of 689 Pa exhibited viscoelastic behavior within the first 100 s. All gels showed elastic behavior 5 min after opening the Epi-tube. In comparison with values in Table 2, gels after evacuation show higher values of Young's modulus which can also be explained by the treatment of a second evacuation step.

To describe the observed viscoelastic behavior, the GKV model (Fig. 1**c**) was chosen as the optimum model for creep modes in a homogeneous viscoelastic solid material. The number of components n in the theoretical model has to correspond to the number of contributors in a real experiment. Since PAAm gels are isotropic and homogenous, n was set to 1. Therefore, only one elastic E_{1_k} and one viscous η_{1_k} elements were chosen for the GKV model. Fitting this model to each creep curve, we calculated values for Young's modulus and viscosity and plotted both values with respect to time in Fig. 5. Decreasing viscosity values down to 0.08 Pa•s can be neglected compared to the high Young's modulus. Therefore, all gels were considered as elastic material after 400 s waiting time before measurements start, as described in chapter 3.3.

5. Conclusion and outlook

We developed a measurement setup to characterize the local viscous, elastic, and viscoelastic properties of soft materials. By using electromagnets in Helmholtz configuration, homogeneous magnetic fields were applied to ferrofluid droplets inside the materials under test. The obtained values for viscosity and elasticity of the materials under test strongly agree with reference values. PAAm gels with the lowest shear modulus of 230 Pa and prepared with evacuation times below 40 min before pouring showed a time-dependent viscoelastic behavior in the first minutes of measurements. For a better understanding of this phenomenon, hydrogels should be synthesized in closed vials with an inert gas atmosphere instead of air in future work. Furthermore, reaction calorimetry and NMR spectroscopy measurements should be carried out to characterize the time-depending polymerization process in detail with regard to oxygen consumption.

The developed setup is robust and can now be deployed to characterize local rheological properties. Of particular interest can be the investigation of local anisotropic as well as time-depending material behaviors. The anisotropies can be characterized by the rotation of the material within the homogeneous magnetic field during testing. The developed setup is an easy to handle and versatile tool.

CRediT authorship contribution statement

Danyil Azarkh: Conceptualization, Investigation, Formal analysis, Data curation, Validation, Visualization, Writing – original draft. **Melanie Geiger**: Investigation, Validation. **Se-Hyeong Jung:** Investigation. **Erik Noetzel**: Supervision, Writing – review & editing. **Rudolf Merkel**: Supervision, Writing – review & editing, Funding acquisition. **Andrij Pich:** Supervision, Writing – review & editing. **Uwe Schnakenberg**: Conceptualization, Writing – original draft, Writing – review & editing, Supervision, Funding acquisition.

Declaration of Competing Interest

The authors declare that they have no known competing financial interests or personal relationships that could have appeared to influence the work reported in this paper.

Data availability

Data will be made available on request.

Acknowledgements

The work was funded by the Deutsche Forschungsgemeinschaft (DFG, German Research Foundation) – 363055819/GRK2415. DA and US express their sincere thanks to Rudolf Leube and Reinhard Windoffer from Institute of Molecular and Cell Anatomy (MOCA) of RWTH Aachen University for using the microscope, to Linda Wetzel for carefully proofreading the manuscript, and to Marc Kunzmann and Stefan Riesner from Quantum Design GmbH (Darmstadt, Germany) for their kind cooperation and carrying out the magnetization measurements of the ferrofluid.

Appendix A. Supporting information

Supplementary data associated with this article can be found in the online version at doi:10.1016/j.sna.2022.113756.

References

[1] D. Roylance, Engineering Viscoelasticity. http://web.mit.edu/course/3/3.11/www/modules/visco.pdf, 2001 (accessed 7 April 2022).
[2] H. Freundlich, W. Seifriz, Über die Elastizität von Solen und Gelen, Z. Phys. Chem. 104 (1922) 223–261, https://doi.org/10.1515/zpch-1923-10415.
[3] P. Kollmannsberger, B. Fabry, High-force magnetic tweezers with force feedback for biological applications, Rev. Sci. Instr. 78 (2007), 114301, https://doi.org/10.1063/1.2804771.
[4] M. Moch, R. Windoffer, N. Schwarz, R. Pohl, A. Omenzetter, U. Schnakenberg, F. Herb, K. Chaisaowong, D. Merhof, L. Ramms, G. Fabris, B. Hoffmann, R. Merkel, R.E. Leube, Effects of plectin depletion on keratin network dynamics and organization, PLoS One 11 (2016), e0149106, https://doi.org/10.1371/journal.pone.0149106.
[5] L. Ramms, G. Fabris, R. Windoffer, N. Schwarz, R. Springer, C. Zhou, J. Lazar, U. Schnakenberg, R. Th. Magin, R. Leube, Merkel, B. Hoffmann, Keratins as main component for the mechanical integrity of keratinocytes, PNAS 110 (2013) 18513–18518, https://doi.org/10.1073/pnas.1313491110.
[6] B.D. Matthews, Electromagnetic needles with submicron pole tip radii for nanomanipulation of biomolecules and living cells, Appl. Phys. Lett. 85 (2004) 2968–2970, https://doi.org/10.1063/1.1802383.
[7] L. Chen, A. Omenzetter, U. Schnakenberg, V. Maybeck, A. Offenhäusser, H.-J. Krause, Passivation of magnetic material used in cell environment, Sens. Actuators B 236 (2016) 85–90, https://doi.org/10.1016/j.snb.2016.04.170.
[8] C. Haber, D. Wirtz, Magnetic tweezers for DNA micromanipulation, Rev. Sci. Instr. 71 (2000) 4561–4570, https://doi.org/10.1063/1.1326056.
[9] B.G. Hosu, K. Jakab, P. Bánki, F.I. Tóth, G. Forgacs, Magnetic tweezers for intracellular applications, Rev. Sci. Instr. 74 (2003) 4158–4163, https://doi.org/10.1063/1.1599066.
[10] A.H.B. de Vries, B.E. Krenn, R. van Driel, V. Subramaniam, J.S. Kanger, Direct observation of nanomechanical properties of chromatin in living cells, Nano Lett. 7 (2007) 1424–1427, https:.//doi.org/10.1021/nl070603+.
[11] L. Chen, A. Offenhäusser, H.-J. Krause, Magnetic tweezers with high permeability electromagnets for fast actuation of magnetic beads, Rev. Sci. Instr. 86 (2015), 044701, https://doi.org/10.1063/1.4916255.
[12] A.H.B. de Vries, J.S. Kanger, B.E. Krenn, R. van Driel, Patterned electroplating of micrometer scale magnetic structures on glass substrates, J. Micro Syst. 13 (2004) 391–395, https://doi.org/10.1109/JMEMS.2004.828724.
[13] Z. Zhang, K. Huang, C.-H. Menq, Design, implementation, and force modeling of quadrupole magnetic tweezers, IEEE/ASME Trans. Mechatron. 15 (2010) 704–713, https://doi.org/10.1109/TMECH.2009.2032179.
[14] J.K. Fisher, J. Cribb, K.V. Desai, L. Vicci, B. Wilde, K. Keller, R.M. Taylor II, J. Haase, K. Bloom, E.T. O'Brien, R. Superfine, Thin-foil magnetic force system for high-numerical-aperture microscopy, Rev. Sci. Instr. 77 (2006), 023702, https://doi.org/10.1063/1.2166509.

[15] U. Banerjee, M. Sabareesh, A.K. Sen, Manipulation of magnetocapillary flow of ferrofluid in a microchannel, Sens. Actuators B 246 (2017) 487–496, https://doi.org/10.1016/j.snb.2017.02.058.
[16] M.A. Bijarchi, A. Favakeh, E. Sedighi, M.B. Shafii, Ferrofluid droplet manipulation using an adjustable alternating magnetic field, Sens. Actuators A 301 (2000), 111753, https://doi.org/10.1016/j.sna.2019.111753.
[17] A. Ray, V.B. Varma, P.J. Jayaneel, N.M. Sudharsan, Z.P. Wang, V. Ramanujana, On demand manipulation of ferrofluid droplets by magnetic fields, Sens. Actuators B 242 (2017) 760–768, https://doi.org/10.1016/j.snb.2016.11.115.
[18] M.A. Bijarchi, M.B. Shafii, Experimental investigation on the dynamics of on-demand ferrofluid drop formation under a pulse-width-modulated nonuniform magnetic field, Langmuir 36 (2020) 7724–7740, https://doi.org/10.1021/acs.langmuir.0c00097.
[19] M.A. Bijarchi, A. Favakeh, M.B. Shafii, The effect of a non-uniform pulse-width modulated magnetic field with different angles on the swinging ferrofluid droplet formation, J. Ind. Eng. Chem. 84 (2020) 106–119, https://doi.org/10.1016/j.jiec.2019.12.026.
[20] M.A. Bijarchi, A. Favakeh, K. Mohammadi, A. Akbari, M.B. Shafii, Ferrofluid droplet breakup process and neck evolution under steady and pulse-width modulated magnetic fields, J. Mol. Liq. 343 (2021), 117536, https://doi.org/10.1016/j.molliq.2021.117536.
[21] M. De Volder, D. Reynaerts, Development of a hybrid ferrofluid seal technology for miniature pneumatic and hydraulic actuators, Sens. Actuators A 152 (2009) 234–240, https://doi.org/10.1016/j.sna.2009.04.010.
[22] B. Andò, A. Ascia, S. Baglio, A. Beninato, The "One drop" ferrofluidic pump with analog control, Sens. Actuators A 156 (2009) 251–256, https://doi.org/10.1016/j.sna.2009.05.006.
[23] H. Hartshorne, C.J. Backhouse, W.E. Lee, Ferrofluid-based microchip pump and valve, Sens. Actuators B 99 (2004) 592–600, https://doi.org/10.1016/j.snb.2004.01.016.
[24] B. Liu, Z. Zhang, J. Yang, J. Yang, D. Li, A rotary ferrofluidic vane micropump with C shape baffle, Sens. Actuators B 263 (2018) 425–458, https://doi.org/10.1016/j.snb.2018.02.113.
[25] K.S. Lok, Y.C. Kwok, P.P.F. Lee, N.T. Nguyen, Ferrofluid plug as valve and actuator for whole-cell PCR on chip, Sens. Actuators B 166–167 (2012) 893–897, https://doi.org/10.1016/j.snb.2012.03.001.
[26] S.M.H. Jayhooni, B. Assadsangabi, K. Takahata, A stepping micromotor based on ferrofluid bearing for side-viewing microendoscope applications, Sens. Actuators A 269 (2018) 258–268, https://doi.org/10.1016/j.sna.2017.11.020.
[27] S. Pal, A. Datta, S. Sen, A. Mukhopdhyay, K. Bandopadhyay, R. Gangulya, Characterization of a ferrofluid-based thermomagnetic pump for microfluidic applications, J. Magn. Magn. Mat. 323 (2011) 2701–2709, https://doi.org/10.1016/j.jmmm.2011.06.016.
[28] B. Assadsangabi, M.S.M. Ali, K. Takahata, Bidirectional actuation of ferrofluid using micropatterned planar coils assisted by bias magnetic fields, Sens. Actuators A 173 (2012) 219–226, https://doi.org/10.1016/j.sna.2011.11.007.
[29] R. Pérez-Castillejos, J.A. Plaza, J. Esteve, P. Losantos, M.C. Acero, C. Cané, F. Serra-Mestres, The use of ferrofluids in micromechanics, Sens. Actuators A 84 (2000) 176–180, https://doi.org/10.1016/S0924-4247(99)00318-0.
[30] B. Andò, S. Baglio, A. Beninato, A ferrofluid inclinometer with a time domain readout strategy, Sens. Actuators A 202 (2013) 57–63, https://doi.org/10.1016/j.sna.2013.02.006.
[31] O. Baltag, D. Costandache, A. Salceanuc, Tilt measurement sensor, Sens. Actuators A 81 (2000) 336–339, https://doi.org/10.1016/S0924-4247(99)00105-3.
[32] B. Andò, S. Baglio, A. Beninato, A flow sensor exploiting magnetic fluids, Sens. Actuators A 189 (2013) 17–23, https://doi.org/10.1016/j.sna.2012.09.026.
[33] B.L. Cheng, L. Yuan, W. Zhu, Y. Song, Hai Xiao, A coaxial cable magnetic field sensor based on ferrofluid filled Fabry-Perot interferometer structure, Sens. Actuators A 257 (2017) 194–197, https://doi.org/10.1016/j.sna.2017.02.024.
[34] R.-J. Yang, H.H. Hou, Y.-N.- Wang, L.-M. Fu, Micro-magnetofluidics in microfluidic systems: a review, Sens. Actuators B 224 (2016) 1–15, https://doi.org/10.1016/j.snb.2015.10.053.
[35] S. Afkhami, A.J. Tyler, Y. Renardy, M. Renardy, T.G. Pierre St., R.C. Woodward, J. S. Riffle, Deformation of a hydrophobic ferrofluid droplet suspended in a viscous medium under uniform magnetic fields, J. Fluid Mech. 663 (2010) 358–384, https://doi.org/10.1017/S0022112010003551.
[36] P. Rowghanian, C.D. Meinhart, O. Campàs, Dynamics of ferrofluid drop deformations under spatially uniform magnetic fields, J. Fluid Mech. 802 (2016) 245–262, https://doi.org/10.1017/jfm.2016.447.
[37] J.C. Bacri, D. Salin, Instability of ferrofluid magnetic drops under magnetic field, J. Phys. Lett. 43 (1982) L649–L654, https://doi.org/10.1051/jphyslet:019820043017064900.
[38] F. Serwane, A. Mongera, P. Rowghanian, D.A. Kealhofer, A.A. Lucio, Z. M. Hockenbery, O. Campàs, In vivo quantification of spatially varying mechanical properties in developing tissues, Nat. Methods 14 (2017) 181–189, https://doi.org/10.1038/nmeth.4101.
[39] A. Serra-Aguila, J.M. Puigoriol-Forcada, G. Reyes, J. Menacho, Viscoelastic models revisited: characteristics and interconversion formulas for generalized Kelvin–Voigt and Maxwell models, Acta Mech. Sin. 35 (2019) 1191–1209, https://doi.org/10.1007/s10409-019-00895-6.
[40] J. Simpson, J. Lane, C. Immer, R. Youngquist, Simple analytic expressions for the magnetic field of a circular current loop, NASA technical documents. ⟨https://ntrs.nasa.gov/api/citations/20010038494/downloads/20010038494.pdf⟩, 2001, (accessed 7 April 2022).
[41] T. Yeung, P.C. Georges, L.A. Flanagan, B. Marg, M. Ortiz, M. Funaki, N. Zahir, W. Ming, V. Weaver, P.A. Janmey, Effects of substrate stiffness on cell morphology, cytoskeletal structure, and adhesion, Cell Motil. Cytoskelet. 60 (2005) 24–34, https://doi.org/10.1002/cm.20041.
[42] Y.L. Jeyachandran, E. Mielczarski, B. Rai, J.A. Mielczarski, Quantitative and qualitative evaluation of adsorption/desorption of bovine serum albumin on hydrophilic and hydrophobic surfaces, Langmuir 25 (2009) 11614–11620, https://doi.org/10.1021/la901453a.
[43] N.-S. Cheng, Formula for the viscosity of a glycerol-water mixture, Ind. Eng. Chem. Res. 47 (2008) 3285–3288, https://doi.org/10.1021/ie071349z.
[44] M.R. Hassan, J. Zhang, C. Wang, Deformation of a ferrofluid droplet in simple shear flows under uniform magnetic fields, Phys. Fluids 30 (2018), 092002, https://doi.org/10.1063/1.5047223.
[45] Y. Aratyn-Schaus, P.W. Oakes, J. Stricker, S.P. Winter, M.L. Gardel, Preparation of complaint matrices for quantifying cellular contraction, J. Vis. Exp. 46 (2010) 2173, https://doi.org/10.3791/2173.
[46] P.H. Mott, C.M. Roland, Limits to Poisson's ratio in isotropic materials, Phys. Rev. B 80 (2009), 132104, https://doi.org/10.1103/PhysRevB.80.132104.
[47] R.E. Rosensweig, Magnetic fluids, Sci. Am. 247 (4) (1982) 136–145, https://doi.org/10.1146/annurev.fl.19.010187.002253.
[48] R. Simič, J. Mandal, K. Thang, N.D. Spencer, Oxygen inhibition of free-radical polymerization is the dominant mechanism behind the "mold effect'' on hydrogels, Soft Matter 17 (2021) 6394–6403, https://doi.org/10.1039/d1sm00395j.
[49] R. Simič, N.D. Spencer, Controlling the friction of gels by regulating interfacial oxygen during polymerization, Tribol. Lett. 69 (2021) 86, https://doi.org/10.1007/s11249-021-01459-1.
[50] https://www.bio-rad.com/webroot/web/pdf/lsr/literature/Bulletin_1156.pdf (accessed 7 April 2022)

Danyil Azarkh studied physics at the National Technical University of Ukraine "Igor Sikorsky Kyiv Polytechnic Institute", Ukraine, and received the M.Sc. degree in 2018. In 2019, he obtained a PhD position at the Institute of Materials in Electrical Engineering 1 (IWE 1) at RWTH Aachen University and is member of the Research Training Group 2415 "Mechanobiology in Epithelial 3D Tissue Constructs (ME3T)" as doctoral researcher.

Melanie Geiger studied molecular and applied Biotechnology at the RWTH Aachen University and received her B.Sc. in 2018. Currently she is working as a research assistant at the Institute for Materials in Electrical Engineering 1 (IWE 1) while continuing her studies at the RWTH Aachen University.

Se-Hyeong Jung studied chemistry at the University of Würzburg, Germany and obtained bachelor degree in 2013. After two years mandatory military service in South Korea, he came back to Germany in 2015 and started his master study at the RWTH Aachen University. In 2017 he finished his study and obtained the master degree in Chemistry from the University. Since 2018, he has been working as PhD student in the research group of Andrij Pich at the DWI – Leibniz institute for Interactive Materials and the RWTH Aachen University, Germany.

Erik Noetzel studied general biology at the RWTH Aachen University, Germany and received his Dipl.-Biol. degree in 2006. After he received his Ph.D. from the same University in 2011, he went to the Forschungszentrum Jülich, Germany, where he worked as a postdoc for five years. Subsequently, he stayed as principal investigator at the Institute IBI-2: Mechanobiology, Forschungszentrum Jülich. At present, he investigates mechanobiological cell signaling circuits between cells, basement membranes and the ECM.

Rudolf Merkel studied general physics at the Technical University Munich, Germany, and received his Dipl.-Phys. degree in 1988. After he received his Ph.D. from the same University in 1993, he went to the University of British Columbia (Vancouver, BC, Canada) where he stayed as a postdoc for two years. Subsequently, he returned to Munich as leader of an independent junior research group. He was appointed as director of an institute at the Forschungszentrum Jülich, Germany, in 2001 and one year later as a full professor in Physical Chemistry at Bonn University, Germany.

Andrij Pich studied chemistry at National University "Lvivska Polytechnika", Lviv, Ukraine and obtained Dipl.-Chem degree in 1996. After he received his PhD and habilitation degree in 2002 and 2008 respectively from the Technical University of Dresden, Germany, he moved to RWTH Aachen University, Germany, with Lichtenberg Professorship funded by Volks0wagenStiftung in 2010. Currently, he is a full professor at the Institute of Technical and Macromolecular Chemistry of RWTH Aachen University and DWI - Leibniz Institute for Interactive Materials.

Uwe Schnakenberg studied physics at University Bonn, Germany, and at RWTH Aachen University, Germany. He worked 10 years with Fraunhofer Institute for Silicon Technology in Berlin, Germany, on innovative microsystem technologies and microsystems. He turned back to RWTH Aachen University working as research director at the Institute of Materials in Electrical Engineering 1 (IWE1) responsible for the development of microsystems for life science applications. In 2003, he received the EUROSENSORS XVII Fellow Award for his contributions in sensor technologies. In 2015, he was appointed as adjunct professor. At present, his interest is on the development of microfluidic systems.

SUPPLEMENTARY INFORMATION

Characterization of Transient Rheological Behavior of Soft Materials Using Ferrofluid Droplets

Danyil Azarkh[1], Melanie Geiger[1], Se-Hyeong Jung[2,3], Erik Noetzel[4], Rudolf Merkel[4], Andrij Pich[2,3,5], Uwe Schnakenberg[1*]

[1] Institute of Materials in Electrical Engineering 1 (IWE1), RWTH Aachen University, Sommerfeldstraße 24, 52074 Aachen, Germany

[2] DWI - Leibniz-Institute for Interactive Materials, Forckenbeckstraße 50, 52074 Aachen, Germany

[3] Institute of Technical and Macromolecular Chemistry, RWTH Aachen University, Worringerweg 2, 52074 Aachen, Germany

[4] Institute of Biological Information Processing (IBI-2): Mechanobiology, Forschungszentrum Jülich GmbH, Leo-Brandt-Strasse, 52425 Jülich, Germany

[5] Aachen Maastricht Institute for Biobased Materials (AMIBM), Maastricht University, Brightlands Chemelot Campus, Urmonderbaan 22, 6167 RD Geleen, The Netherlands

* Corresponding author, schnakenberg@iwe1.rwth-aachen.de

Preparation of 2 % (w/v) methylcellulose

For the preparation of 2 % (w/v) methylcellulose/water solution 1/3 of 150 mL DI water was filled in a fresh beaker. The remaining 2/3 of the water was cooled down in ice water. The first water part was heated to 80 °C. 3 g of methylcellulose powder (Sigma Aldrich) was added to the hot water accompanied by continuous stirring until it was homogeneously mixed. With continuous stirring, the heat was turned off, the remaining cold water was added and the whole solution was transferred to another beaker, which was prepared with ice. The solution was stirred for more 15 minutes in ice to cool down and then transferred to a fridge for further use. Before use, the solution was warmed up in closed glass to room temperature.

Preparation of polyacrylamide (PAAm) gels

The stock solutions for the PAAm gels with shear moduli G of 230 Pa, 689 Pa and 1535 Pa were prepared according to Aratyn-Schaus et al. [41]. 40 % (w/v) acrylamide (1610140, BioRad), 2 % (w/v) bis-acrylamide (1610142, BioRad), and deionized (DI) water were mixed according **Table A.1**. The appropriate stock solution was evacuated in a vacuum chamber for 20 min. From the stock solution, the working solution was prepared by mixing DI-water, 10 % (w/v) ammonium persulfate (APS) (1610700, BioRad) and tetramethylethylenediamine (TEMED) (1610800, BioRad) in ratios as mentioned in **Table A.1**. The working solution was tightly mixed by sucking and pushing the solution with an Eppendorf pipette. The appropriate solution was divided into five equal volume parts. For gelation, the parts were transferred to Eppendorf Safe-Lock tubes. The closed Eppendorf Safe-Lock tubes were turned upside-down to achieve flat gel surfaces on one side by characterization of the gels later in the light microscope. After 24 h of gelation time, the tubes were opened and the gels were deposited with their flat surfaces on the glass slide for the measurements.

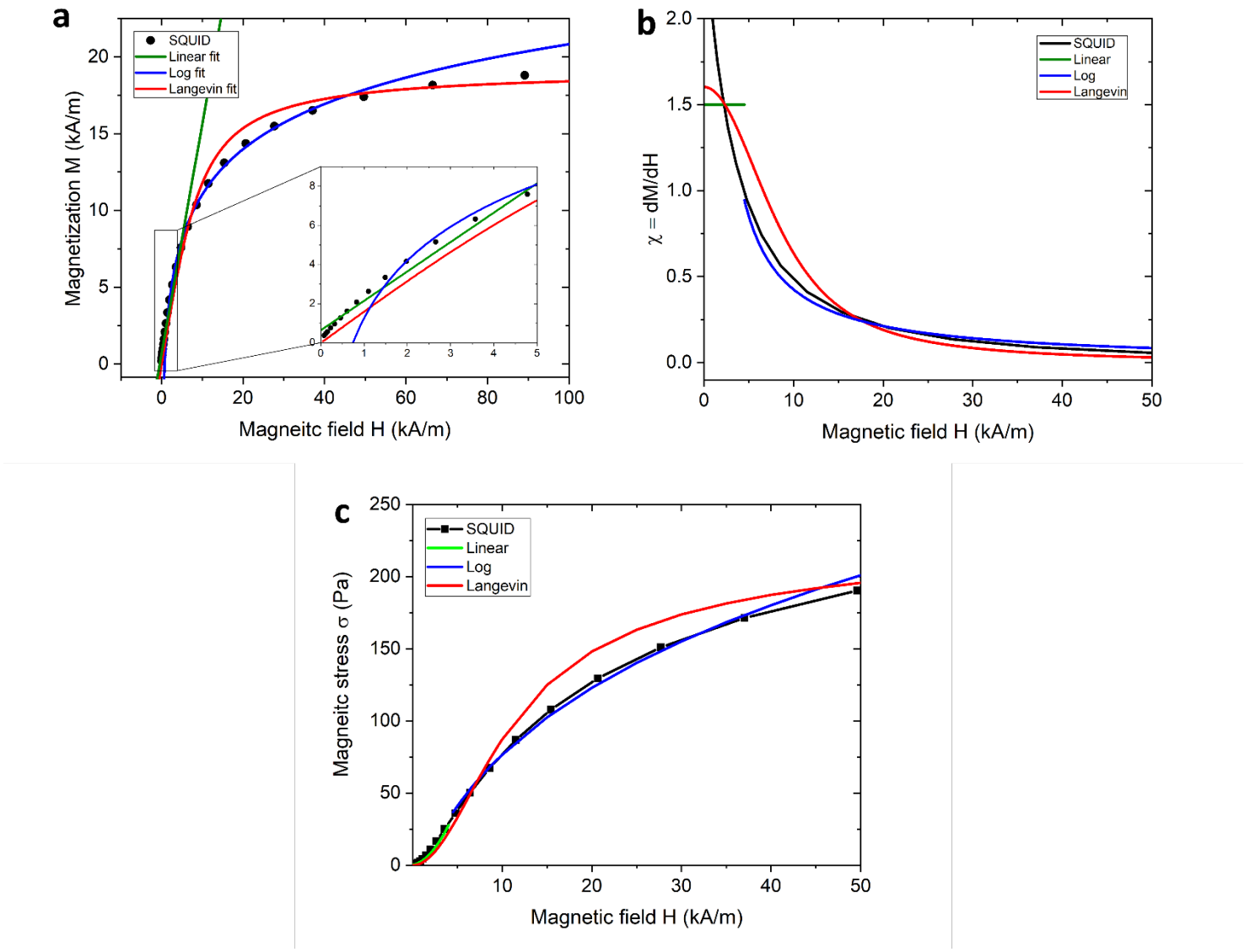

Fig. A.1: Magnetization of ferrofluid. Black dots indicate SQUID measurements with the PPMS-DynaCool magnetometer (Quantum Design). The green line represents linear fitting $y(x) = 1.5\,x + 650$ for the low magnetic field range, the blue line the logarithmic fit with function $y(x) = 4250\ln(x) - 28100$ and red line the Langevin fit $M_{lan} = \varphi M_d\, L(\alpha)$, where $\varphi = 0.043$ is volume fraction, $M_d = 446000$ A/m the magnetic domain magnetization of magnetite and $L(\alpha) = \coth\alpha - 1/\alpha$ the Langevin function. Here $\alpha = \frac{\pi\mu_0 M_d H d^3}{6kT}$ with $k = 1.38 \times 10^{-23}\ N\,m/K$ the Boltzmann constant, $T = 293.15\ K$ the temperature, $\mu_0 = 4\pi \times 10^{-7}$H/m the permeability of free space, $d = 11\ \mu m$ the average particle size, and H the applied external magnetic field strength in A/m, respectively. **(a)** Magnetization M of ferrofluid with regard to the applied magnetic field H. The inset shows the low field magnetization range from 0 to 5 kA/m. The crossover point between linear and logarithmic magnetization behavior was determined from equating the logarithmic and the linear function, yielding a field of H = 4919 A/m for the crossover from linear to logarithmic regime. **(b)** Magnetic susceptibilities of ferrofluid $\chi = dM/dH$ with respect to magnetic field strength H for the measurement and fitting curves. **(c)** Dependency of magnetic stresses $\sigma = \mu_0 M(H)^2/2$ on magnetic field strength H with respect to different magnetization $M(H)$ for the measurement and fitting curves.

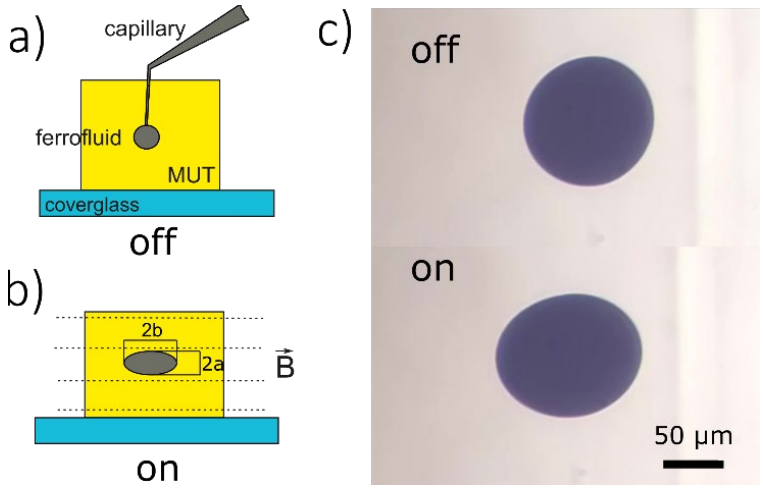

Fig. A.2: Scheme of injection of a ferrofluid droplet into the MUT: **a)** magnetic field off **b)** magnetic field on. *a* and *b* represent minor and major droplet radius under deformation, respectively. Drawing not to scale; **c)** Photograph of a ferrofluid droplet in glycerin 99.95 % (v/v) without (off) and with (on) magnetic field.

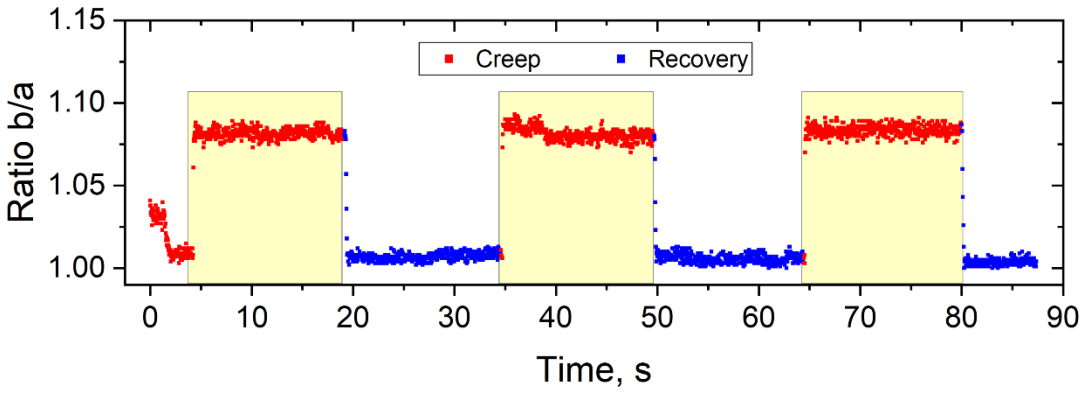

Fig. A.3: Ferrofluid droplet deformation in glycerin 99.95 % (v/v): Measured droplet radii ratios b/a plotted over time. In the relaxed state, a slight droplet deformation was measured in general, which was also reported by [38]. The small offset resulted from image analysis functions in Matlab that convert a color picture to black and white and then calculate the droplet size from pixels number of the black droplet.

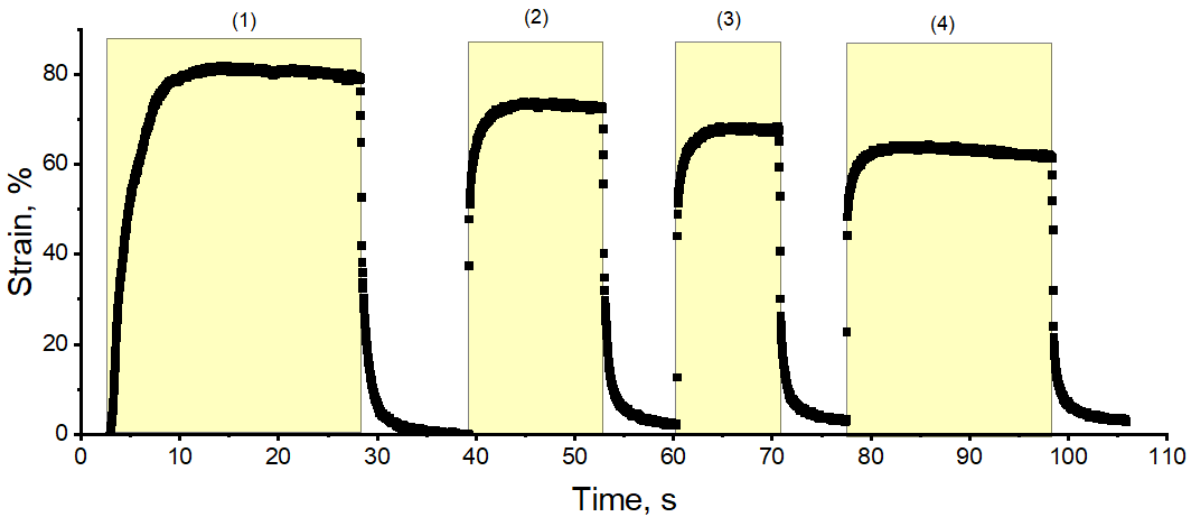

Fig. A.4 Time dependency of strain of PAAm gel with a shear modulus G of 230 Pa for the first four periods of magnetic field applied shortly after preparation. The yellow rectangles show the time slots of applied magnetic stress (40 Pa). In the relaxed state, a slight droplet deformation was measured in general, which was also reported by [38].

Table A.1: PAAm stock and working solutions

Shear Modulus G, Pa	**230**	**689**	**1535**
Stock Solution			
40 % (w/v) Acrylamide, mL	1.25	3.12	2.34
2 % (w/v) Bisacrylamide, mL	0.5	0.083	0.188
Water, mL	3.25	1.797	2.472
Total, mL	5	5	5
Working solutions			
Stock solution, µL	300	300	400
Water, µL	693.5	693.5	593.5
TEMED, µL	1.5	1.5	1.5
10 % (w/v) APS, µL	5	5	5
Total, µL	1000	1000	1000
Final concentration ratio Acrylamide / Bisacrylamide	3 / 0.06	7.5 / 0.01	7.5 / 0.03

Table A.2: Fitting data to curves in Fig. 4b

Equation	$\boldsymbol{\sigma = E_A \varepsilon}$				
Plot	**12 µm**	**25 µm**	**37 µm**	**40 µm**	**45 µm**
Slope	755 ± 35	709 ± 5.9	439± 3.7	415± 4.3	259± 2
R_s^2	0.94756	0.99006	0.98898	0.98465	0.99089

Table A.3: Fitting data to three curves in Fig. 4c

Plot	**PAAm** G **= 230 Pa**	**PAAm** G **= 689 Pa**	**PAAm** G **= 1535 Pa**
Intercept	70 ± 6.8	206 ± 12.95	144 ± 22.5
Slope	$0.0063 \pm 2 \cdot 10^{-5}$	$0.0073 \pm 5.3 \cdot 10^{-5}$	$0.0166 \pm 1.25 \cdot 10^{-4}$
$\mathbf{R_s^2}$	0.99449	0.99425	0.99805

Fitting data in Tables A.2 and A.3 were obtained using software OriginPro 2018 (OriginLab Corporation, Northampton, MA, USA).